Hindawi
Advances in Polymer Technology
Volume 2022, Article ID 5780884, 13 pages
https://doi.org/10.1155/2022/5780884

Research Article

Effect of MoS_2 Yolk-Shell Nanostructure on the Thiophene Separation Performance of PEG Membrane

Ziman Hou,[1] **Ping Peng**,[1,2] **Yongqiang Lan**,[1] **Zihui Wu**,[1] **and Jianhua Wang**[1,2]

[1]*Laboratory of Membrane Science and Technology, School of Resource and Chemical Engineering, Sanming University, Sanming, Fujian, China 365004*
[2]*Science and Technology on Sanming Institute of Fluorochemical Industry, Sanming, Fujian, China 365004*

Correspondence should be addressed to Ping Peng; mailpengping@sina.com and Yongqiang Lan; lanyongqiang@hotmail.com

Received 22 January 2022; Revised 28 June 2022; Accepted 14 July 2022; Published 27 July 2022

Academic Editor: Júlio Santos

Constructing facilitated transport based on π-complexation has been drawing more and more attention in mixed matrix membranes (MMMs) for pervaporative desulfurization. Herein, a unique molybdenum disulfide (MoS_2) yolk-shell nanostructure (MYNS) was prepared and incorporated into the polyethylene glycol (PEG) matrix to fabricate MMMs for model gasoline desulfurization by PV. Moreover, the effects of MYNS content, feed sulfur concentration, and feed temperature on the performance of PEG/MYNS MMMs were evaluated. It was found that there is good interfacial compatibility between the MYNS filler and the PEG matrix, and the resultant MMMs show enhanced swelling resistance against thiophene. The PV results revealed that the as-fabricated MMMs are thiophene-selective, and their desulfurization performance in the pervaporative removal of thiophene from *n*-octane is remarkably evaluated due to the addition of MYNS. The MMMs display the highest sulfur enrichment factor of 4.02 with an associated permeation flux of 2587 $g \cdot m^{-2} \cdot h^{-1}$ with the MYNS loading of 3 wt. % when carrying out in an *n*-octane and thiophene (500 $\mu g \cdot g^{-1}$) mixture at 343 K. Furthermore, a consistent increment in the permeation flux accompanied with a continuous reduction in the enrichment factor was observed with increasing the feed sulfur concentration and feed temperature. This work may offer great potential for practical gasoline desulfurization applications.

1. Introduction

With the increasing environmental pollution, people have put more stringent requirements on the sulfur content in petroleum products. The deep desulfurization of fuel has become a very important issue in the oil refining industry [1, 2]. Until now, the most commonly used desulfurization technology is hydrodesulfurization (HDS). However, the HDS process is high cost due to high temperature, high pressure, and high hydrogen consumption and results in a significant loss in gasoline octane number [3]. Moreover, it provides a very efficacious method for separating thiols and sulfides in gasoline except thiophene. Thiophene is the main sulfur-containing compound in gasoline, accounting for about 60-80% of the total sulfur content [4, 5]. Consequently, it is desirable to explore other lower cost and high efficiency desulfurization methods.

Pervaporation (PV) desulfurization technology has received more and more attention worldwide [6]. Compared with traditional desulfurization technology, it has many potential advantages, including low energy consumption, low pollution, high separation efficiency, and simple equipment [3, 6–9]. In recent years, there are a large number of investigations on photovoltaic gasoline desulfurization. Most studies focus on introducing processes, amplifying technology, exploring membrane materials, optimizing operation parameters, etc. [10–14]. Recent attempts have focused on membrane modification in order to improve the separation performance [7]. Introducing adsorptive fillers into polymer matrices is an effective and flexible approach to enhance the desulfurization performance of membranes by improving the adsorption capacity of the target permeate components. To date, many adsorbents, such as metal oxides, zeolite, and activated carbon, have been adopted for the desulfurization of gasoline [13, 15, 16].

Transition metal sulfides, which are similar to graphene in structure, have attracted much attention due to their special optical, electrical, and chemical properties. Two-dimensional (2D) layered molybdenum disulfide (MoS_2) exhibits specific photoelectric, catalytic, biological, and energy harvesting properties [17]. The direct band gap of monolayer MoS_2 reaches 1.8 eV, showing light absorption and photoluminescence characteristics [18, 19]. Therefore, MoS_2 has many unique optical and physical and chemical properties and is widely used in photocatalysis, energy, electronic chips, biological detection, medical imaging, and other fields [20]. Recently, researchers have employed 2D materials (graphene and its derivatives and MoS_2 nanosheets) with high specific surface area as well as adjustable interlayer spacing as fillers to prepare MMMs. The functional groups available on the 2D nanosheet surface, which are used as facilitated transport carriers for thiophene, can effectively improve the PV desulfurization efficiency of membranes [21–23]. The reasons are the following two attributes: (i) the polymer chain packing is disrupted by the addition of 2D materials with a high aspect ratio which provides more diffusion pathways; (ii) the specific and reversible π-π interaction between the facilitated transport carriers and thiophene molecules results in a faster diffusion rate of thiophene and an increase of the overall selectivity towards thiophene [21, 23]. However, the MMMs prepared by incorporating 2D materials have some drawbacks. Due to the poor compatibility between the 2D materials and the polymer materials, the performance of the MMMs is poor, including poor separation performance, low swelling resistance, and poor stability.

In this work, a MoS_2 yolk-shell nanostructure (MYNS) was prepared. MoS_2 was encapsulated in hollow mesoporous carbon nanosheets like a photo in a plastic bag. This three-dimensional (3D) structure combines the advantages of 2D ultra-thin nanostructure and hollow porous nanostructure and can overcome the inherent defect of poor compatibility between traditional 2D materials and polymer materials. The MYNS was incorporated as fillers in polyethylene glycol (PEG) to prepare MMMs for improving the desulfurization performance via PV. The thus-prepared MMMs were utilized for the removal of thiophene from *n*-octane. Thanks to the high surface area, large pore volume, and excellent dispersion of the MYNS, the PEG/MYNS MMMs showed enhanced desulfurization performance. Also, the effects of the content of MYNS, feed sulfur concentration, and operating temperature on the separation performance were analyzed systematically.

2. Materials and Methods

2.1. Materials. Polyvinylpyrrolidone (K13-18) and PEG (number-average molecular weight~20,000) were obtained from Shanghai Aladdin Biochemical Technology Co., Ltd. Ethanol, 1-methyl-2-pyrrolidone, ethylenediamine, ammonia solution (28% in water), resorcinol, formaldehyde solution, maleic anhydride, *n*-octane, and hydrofluoric acid were purchased from Sinopharm Chemical Reagent Co., Ltd. Thiophene, trimethylamine solution (33% in ethanol), MoS_2, and tetraethyl orthosilicate were acquired from Shanghai Macklin Biochemical Co., Ltd. Polyvinylidene fluoride (PVDF) microfiltration membranes (average pore size 0.45 μm) were used as porous support and were provided by Tianjin Jinhai Environmental Monitoring Material Manufacturing Co., Ltd. All chemicals were of analytical reagent (AR) grade and used without any purification.

2.2. Synthesis of MYNS. First, 30 mg MoS_2 nanosheets were dispersed in a 135 mL ethanol and water mixture (volume ratio = 8 : 1) under ultrasound for 10 min at 30°C. Subsequently, the dispersion was mixed with 0.3 g polyvinylpyrrolidone, 6 mL ammonia solution, and 4 mL tetraethyl orthosilicate. After stirring thereafter for 6 hours, centrifugation was used to collect the MoS_2@silica (SiO_2) products, followed by washing with deionized water. The precipitation was dispersed into 30 mL deionized water. After that, the dispersion was combined with a 270 mL ethanol and water mixture (volume ratio = 1 : 2). After mixing with 1.8 mL tetraethyl orthosilicate, 0.9 mL formaldehyde, 0.6 g resorcinol, and 0.9 mL ethylenediamine, the mixture was left to stir at 40°C for one day. The dispersion was centrifuged, and the resultant intermediate MoS_2@SiO_2@carbon precursor polybenzoxazine (PB) was dried at 60°C over 12 hours. After carbonization at 800°C for 4 hours in a nitrogen (N_2) atmosphere, the obtained was washed with a 10% hydrofluoric acid solution for one day. Eventually, the resulting dispersion was centrifuged and washed with deionized water. The desired final product MYNS was obtained after further drying under vacuum overnight.

2.3. Membrane Preparation. The polymer PEG and the filler MYNS were mixed with the solvent 1-methyl-2-pyrrolidone. After adding the crosslinking agent maleic anhydride and the catalyst trimethylamine solution, the mixture was left to stir for 50 minutes. After degasification, the dope solution was cast on the PVDF support that had been immersed into deionized water for 3 more hours prior to casting to prevent dope solutions from penetrating. The as-prepared membranes were introduced into an oven at 90°C to allow for vaporization of the solvent and complete crosslinking, followed by drying in a vacuum oven for 24 hours at room temperature to ensure removal of residual solvent. The method for the preparation of the membrane samples that were used for sorption experiments was pouring the casting solution into Petri dishes instead of PVDF membranes.

2.4. Characterizations. The chemical compositions of MYNS and PEG/MYNS MMMs were determined with a Fourier transform infrared spectrometer (FTIR, Spectrum 65 FT-IR Spectrometer, Perkin Elmer and VERTEX 70, Bruker). The crystal structure of MYNS was characterized by an X-ray diffractometer (XRD, X'Pert Pro MPD, PANalytical) using Cu Kα radiation ($\lambda = 0.154$ nm). A scanning electron microscope (SEM, Helios G4 CX, FEI) was used for observing the surface morphology of MYNS particles and the surface and cross-section morphologies of PEG/MYNS MMMs. The surface chemical composition of the MYNS was characterized by X-ray photoelectron spectroscopy (XPS, PHI 550

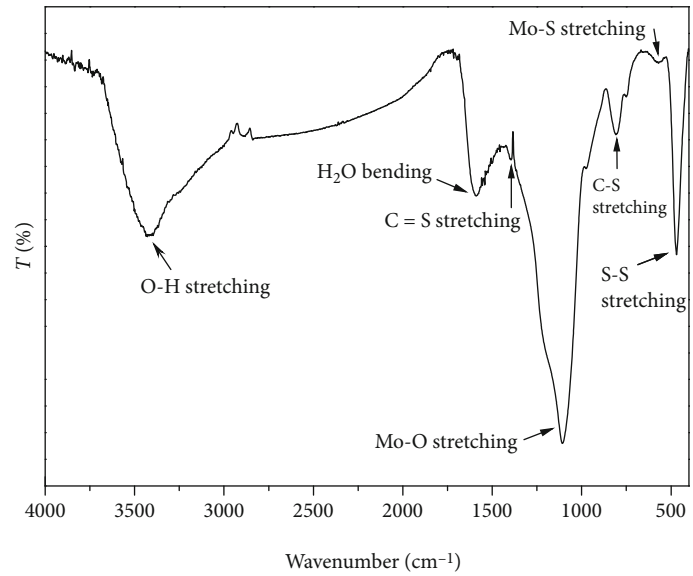

Figure 1: FTIR spectrum of MYNS.

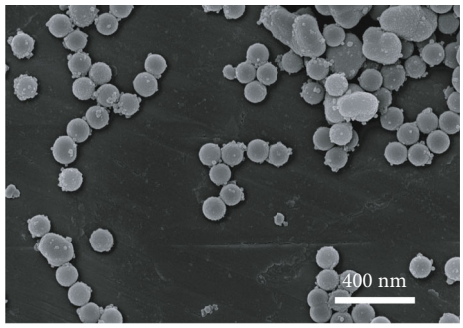

Figure 2: SEM image of MYNS.

ESCA, Perkin Elmer) using Mg Kα radiation source ($h\upsilon$ = 1253.6 eV). A homemade scanning tunneling microscopy (STM)/atomic force microscopy (AFM) system was applied to measure the surface roughness of membranes under an atmosphere of N_2 at room temperature. For assessing the thermal stability of membranes, the thermal gravimetric analysis (TGA) was conducted on a simultaneous thermal analyzer (STA 449 F3 Jupiter) in a temperature range from 30 to 800°C at a heating rate of 10°C·min^{-1} in a N_2 atmosphere. Sorption experiments were performed to evaluate the membrane swelling degree. The free-standing membrane samples were dried at 80°C in a vacuum oven for approximately 3 days, and their weights were recorded. Subsequently, they were immersed completely into thiophene solution and were left to soak for 48 hours at room temperature to achieve adsorption equilibrium. After that, the samples were removed and quickly wiped the excess solvent from their surface with filter papers and then weighed immediately. The swelling degree, SD, can be calculated as

$$\mathrm{SD} = \frac{W_s - W_d}{W_d} \times 100\%, \quad (1)$$

in which W_d and W_s represent the weights of initial dried and final swollen membrane samples, respectively. Three samples of each membrane were tested.

2.5. PV Experiments. PV experiments were made on the self-designed apparatus described in our previous work [24]. The feed mixture was a model gasoline system composed of *n*-octane and thiophene, and the thiophene concentration was controlled in the range of 500-1700 μg·g^{-1}. Feed solutions were stirred constantly using a submerged pump to eliminate the concentration polarization. A recirculating water bath was used to realize the stable control of the feed temperature ranging from 343 to 383 K. Permeates were trapped by combining purging with nitrogen and vacuuming and keeping the pressure below 20 kPa. The pervaporative desulfurization performance can be expressed in terms of the permeation flux (J, g·m^{-2}·h^{-1}) and the enrichment factor (β) which are calculated as follows:

$$J = \frac{Q}{At}, \quad (2)$$

$$\beta = \frac{\omega_P}{\omega_F}, \quad (3)$$

where Q is the weight of the permeate, A refers to the effective membrane area, and t represents the experiment time, respectively. ω_F and ω_P refer to the weight fractions of thiophene in the feed and permeate, respectively. The composition of the permeate was measured by gas chromatography-mass spectrometry (GC-MS, 5977B GC/MSD, Agilent).

3. Results and Discussion

3.1. Characterization of MYNS. The FTIR spectrum of the MYNS is represented in Figure 1. A strong peak at around 3425 cm^{-1} is attributable to O–H stretching, which is due to the adsorption of water on the MYNS surface [25]. The absorption peak at 1590 cm^{-1} can be attributed to the

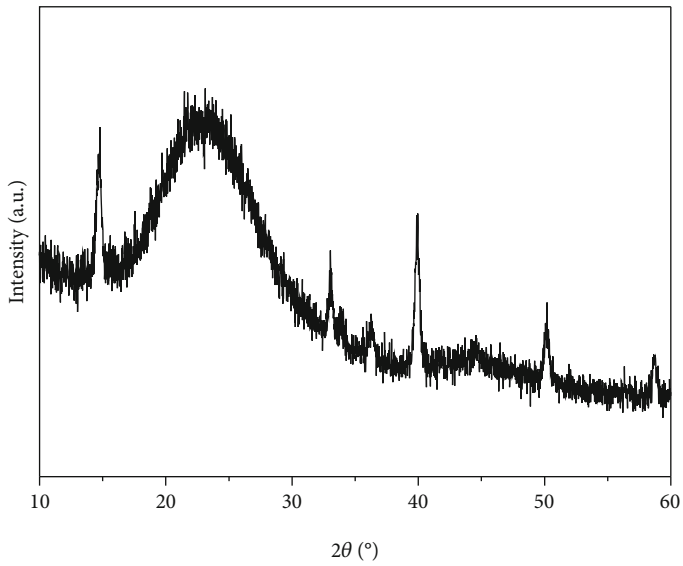

Figure 3: XRD spectrum of MYNS.

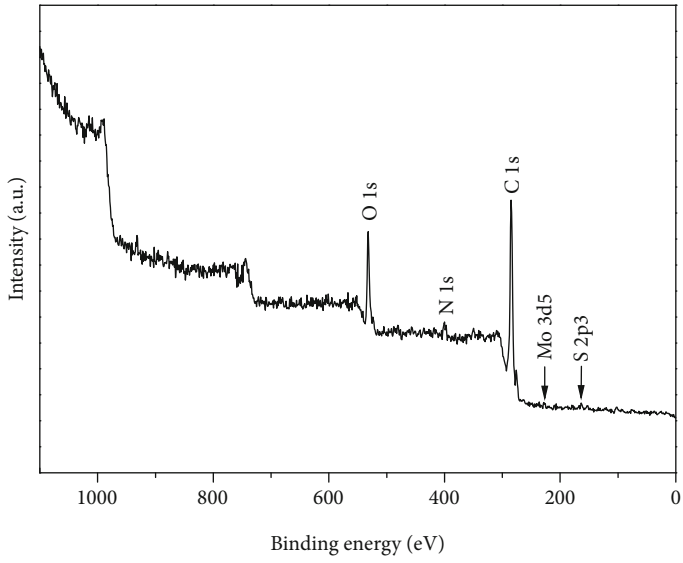

Figure 4: XPS spectrum of MYNS.

bending of the water molecule. The characteristic peak at 469 cm^{-1} arises from S–S stretching vibration in MoS_2 [26]. The weak peak at 535 cm^{-1} and the strong peak at 1107 cm^{-1} are assigned to Mo–S and Mo–O stretching, respectively. The characteristic peak at 809 cm^{-1} corresponds to C–S stretching [27]. In addition, a weak absorption peak can be observed at 1395 cm^{-1}, which belongs to the stretching of C=S bond [28], indicating the formation of chemical bonds between the MoS_2 and the porous carbon coated on it. It is suggested that the prepared MYNS has high structural stability. It is worth noting that typical characteristic peaks of SiO_2 are not shown in the spectrum. That is because the middle SiO_2 layer of the intermediate MoS_2@-SiO_2@PB was completely removed by etching with the hydrofluoric acid solution. It is concluded that the yolk-shell nanoarchitecture of MYNS, MoS_2, and carbon with rich nanopores was successfully prepared.

Figure 2 shows the morphology of the MYNS particles. In Figure 2, it can be observed that MYNS particles are basically spherical and have an average size of approximately 100 nm with uniform size distribution. Nanoscale MYNS particles as filler are instructive in obtaining defect-free MMMs and evaluating membrane separation performance in PV. Besides, it is also can be seen that the SEM image of MYNS shows fewer agglomerates, and the MYNS particles are almost monodisperse. MYNS is expected to be well

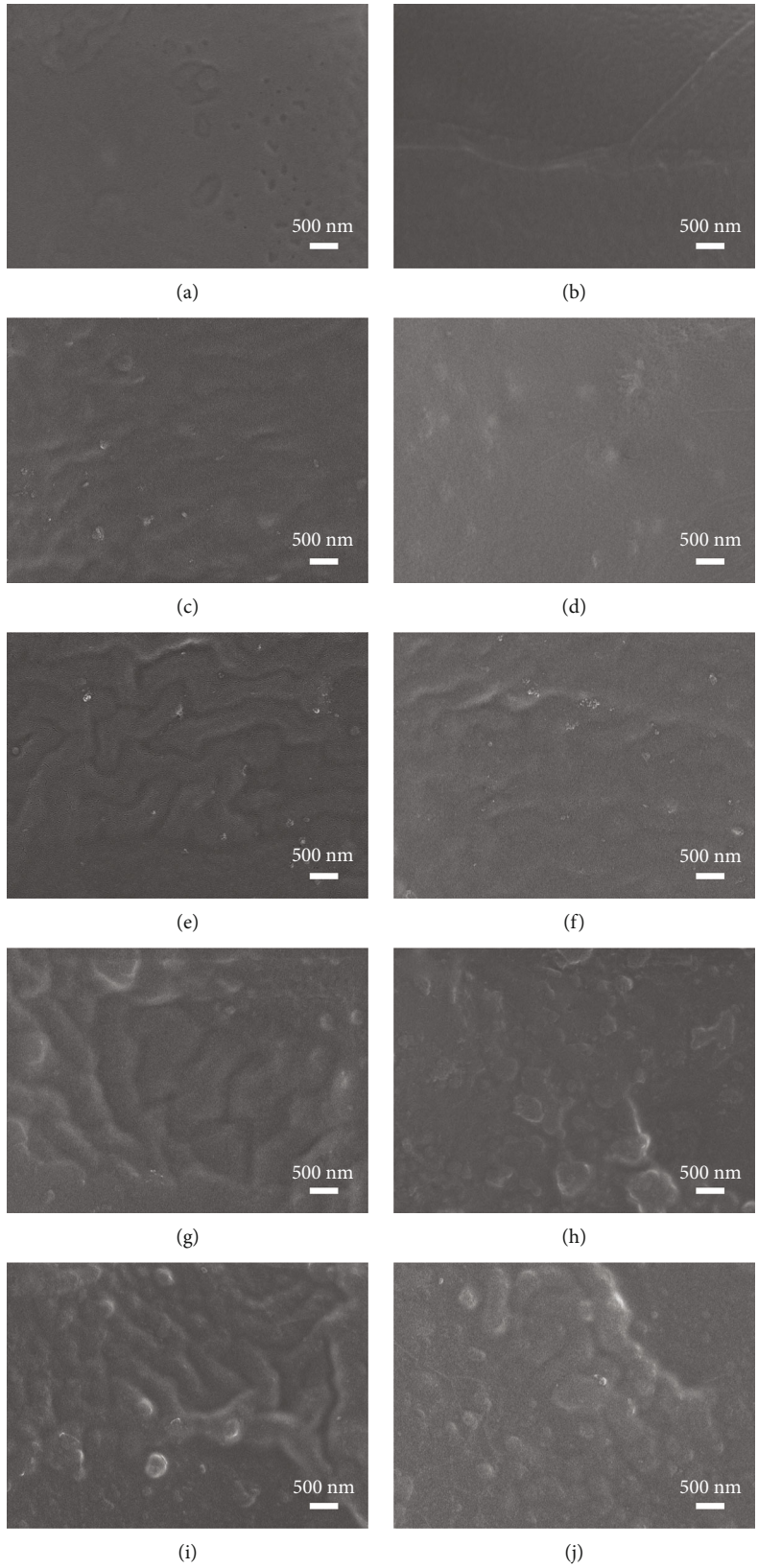

Figure 5: Continued.

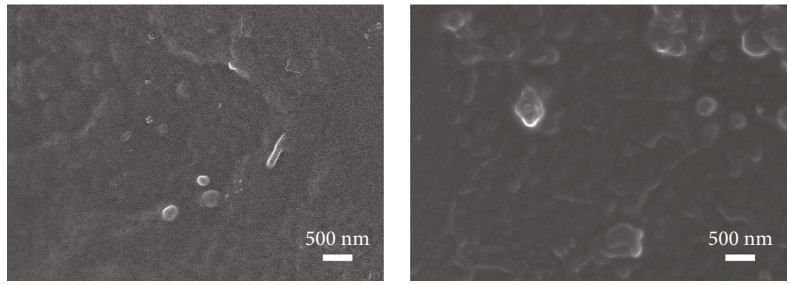

Figure 5: Surface and cross-sectional SEM images of PEG/MYNS MMMs with different MYNS contents: (a, b) 0, (c, d) 1, (e, f) 2, (g, h) 3, (i, j) 4, and (k, l) 5 wt. %.

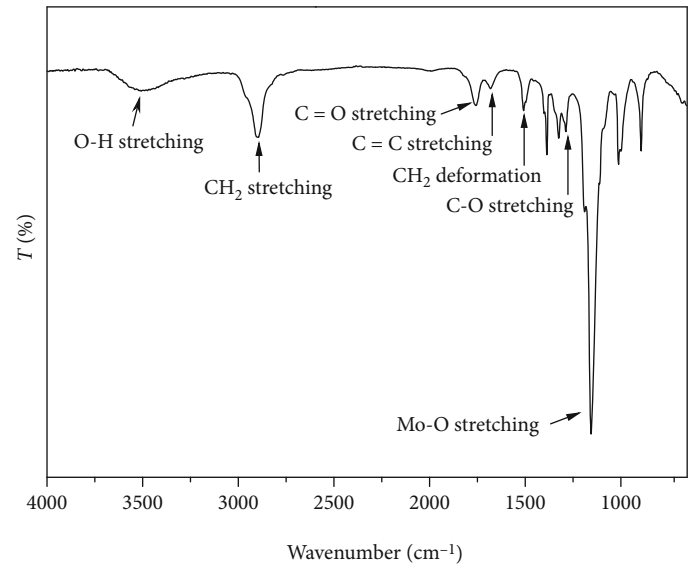

Figure 6: FTIR spectrum of PEG/MYNS MMM.

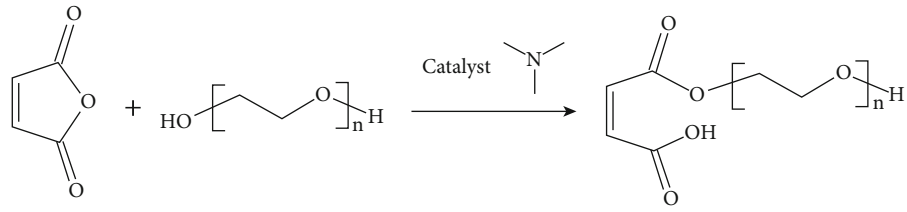

Scheme 1: Schematic representation of the crosslinking reaction of PEG with maleic anhydride.

dispersed in the PEG matrix, reducing the formation of undesirable nonselective voids at the interface between them, hence yielding an escalating thiophene perm-selectivity.

Figure 3 represents the XRD pattern of MYNS. A broad diffraction peak 2θ of about 23° and a weak diffraction peak at 2θ of near 44° are the classic characteristic peaks of (002) and (100) crystal planes of carbon materials, thereby confirming the presence of carbon structure in the resultant MYNS. Moreover, the diffraction peaks at $2\theta = 14.8°$, 33.0°, 39.9°, 50.1°, and 58.6° can be designated in the (002), (100), (103), (105), and (110) single crystal planes for MoS_2 [27], which are basically in accordance with those of typical MoS_2 crystal (JCPDS Card No.37-1492), demonstrating the existence of MoS_2 in the MYNS.

Figure 4 shows the XPS spectrum of MYNS over the binding energy range of 0-1100 eV that was calibrated by the C 1 s peak at 284.8 eV. From the full element survey, peaks of oxygen, nitrogen, carbon, molybdenum, and sulfur are observed, and the percentages of corresponding components are accordingly calculated to be 12.85, 4.07, 82.19, 0.20, and 0.69, respectively. This demonstrates that carbon

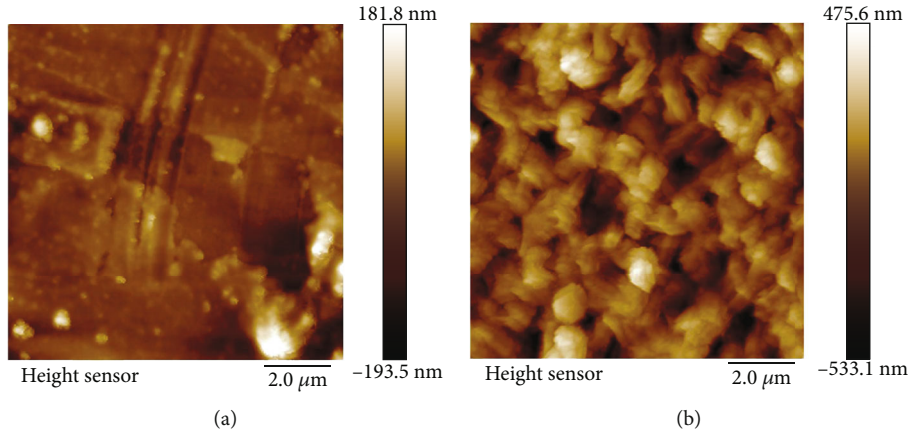

Figure 7: AFM images of (a) PEG membrane and (b) PEG/MYNS MMM.

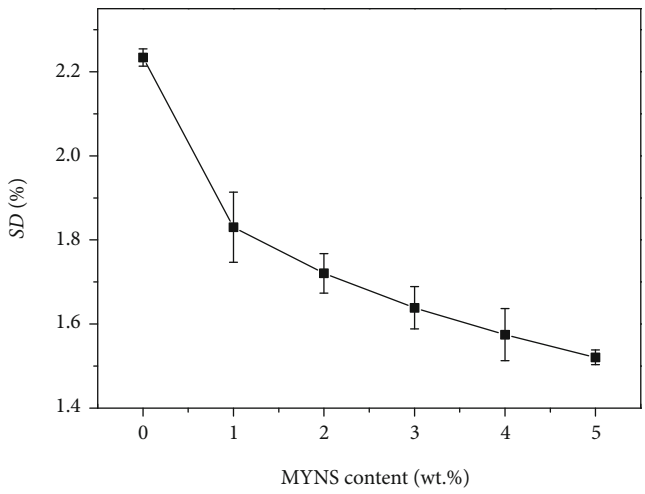

Figure 8: Swelling degree of PEG and PEG/MYNS membranes with different MYNS contents in thiophene.

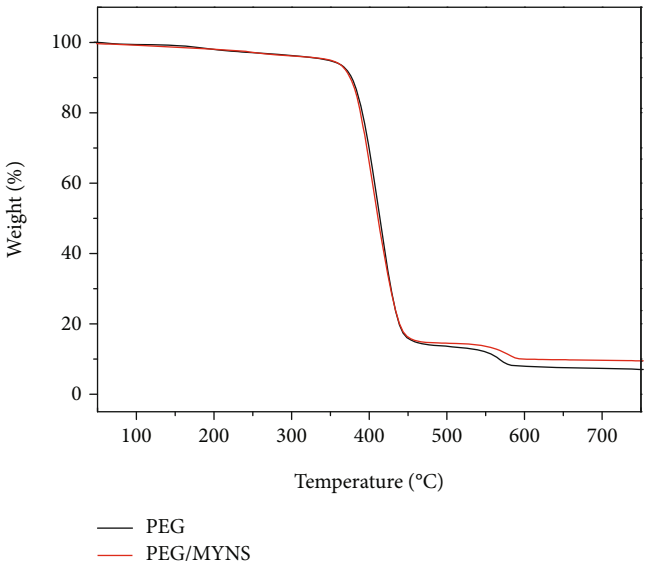

Figure 9: TGA curves of PEG and PEG/MYNS membranes.

was wrapped on the MoS_2 surface, forming the yolk-shell structure.

3.2. Characterization of Membranes. Figure 5 presents the surface and cross-sectional morphologies of the pure PEG membrane and PEG/MYNS MMMs with different MYNS loading ranged in 1-5 wt. %. From the surface SEM images listed in the first column, it is noticeable that the pure PEG membrane surface is smooth and dense, and the PEG/MYNS membrane surface becomes rough and uneven with increasing the MYNS loading. No pinholes or obvious cracks are found on the surface of all the membranes, which is important for membrane separation. From the cross-sectional SEM images displayed in the second column, it can be found that the interface between MYNS fillers and PEG matrix is indistinct, indicating good interfacial compatibility between them. It is worth mentioning that MYNS still disperses well within the PEG matrix even when the MYNS loading is up to 3 wt. %. However, excessive filler aggregation is evident both on the membrane surface and in the membrane with the further increase of the MYNS loading (over 3 wt. %), inducing the formation of nonselective defects, hence resulting in the degradation of separation performance.

The ATR FTIR spectrum of the PEG/MYNS MMM with 3 wt. % MYNS is presented in Figure 6. A weak absorption band at around 3500 cm^{-1}, which is characteristic of, is designated to hydroxyl (–OH) groups. The peaks at 2877 and 1467 cm^{-1} are characteristic for methylene ($–CH_2$) stretching and deformation vibration, respectively. The peaks at 1642 and 1242 cm^{-1} belong to C=C and C–O stretching vibrations, respectively. It is noted that the representative two absorbances at around 1800 and 1750 cm^{-1} originated from the stretching vibration of two neighboring carbonyl (C=O) groups of maleic anhydride are not observed in the spectrum. Conversely, an absorption peak at 1720 cm^{-1} related to C=O stretching vibration appears. It is indicated that the crosslinking reaction occurs between PEG and maleic anhydride. The schematic representation of the crosslinking reaction is shown in Scheme 1. The strong peak at 1107 cm^{-1} displayed in the spectrum proves the presence of MYNS.

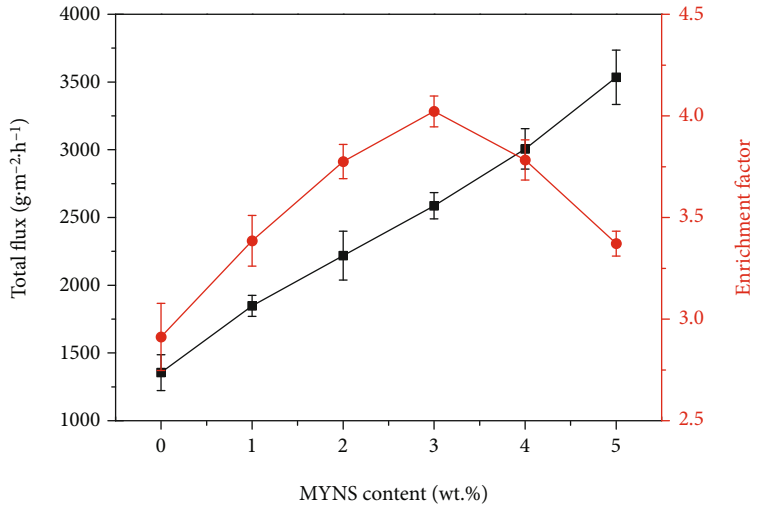

Figure 10: Effect of MYNS content on desulfurization performance.

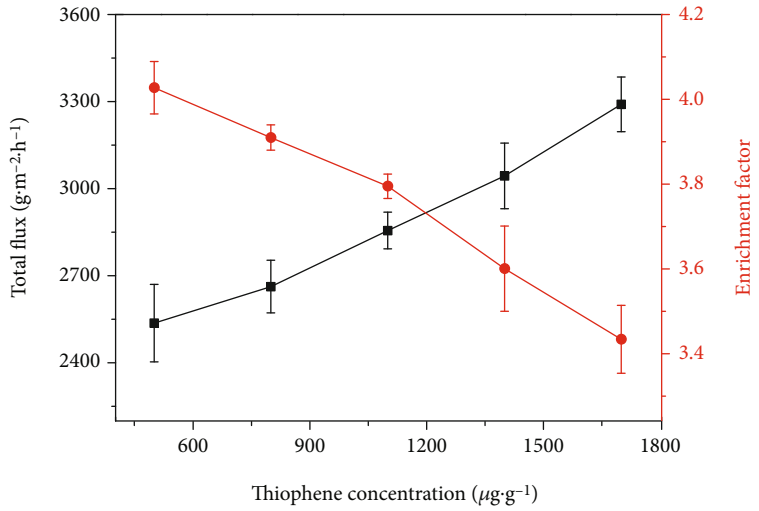

Figure 11: Effect of thiophene concentration in feed on desulfurization performance of PEG/MYNS MMMs.

Figure 7 shows the AFM images of the pristine PEG membrane and the PEG/MYNS MMM filled with an MYNS loading of 3 wt. %, respectively. The surface roughness of the pristine PEG membrane is 35.2 nm, while it is 141 nm for the PEG/MYNS MMM. It is indicated that the addition of MYNS into the PEG led to the increase in the membrane surface roughness, inferring the increase of the membrane surface area. A study reported by Wu et al. [16] demonstrated that the membrane surface area has a positive correlation with the permeation flux. From this point of view, incorporating MYNS into the PEG will evidently improve the membrane permeation flux.

The swelling degree of as-fabricated pure PEG and PEG/MYNS membranes with different MYNS contents was tested in thiophene, and the obtained results are given in Figure 8. A large reduction in the swelling degree for all the MYNS filled PEG MMMs is found as compared with the PEG pristine membrane, which indicates a higher antiswelling capacity of PEG membranes towards thiophene due to the incorporation of MYNS. Furthermore, the swelling resistance increases as the MYNS content increases. According to the study reported by Gonciaruk et al. [29], the introduction of MYNS into PEG has an effect on the polymer chain packing. The PEG chain fragments are arranged parallel to the MYNS sheets, leading to a decrease in the chain mobility and potentially preventing the membrane from swelling. The high swelling resistance in the desulfurization can ensure high performance stability during a long-term operation which is crucial in practical applications.

Thermal stability of the pure PEG membrane and PEG/MYNS MMM with an MYNS loading of 3 wt. % was tested by TGA, and the resulting thermograms are presented in Figure 9. It can be found that the two weight loss curves exhibit a similar thermal degradation trend, confirming little influence on the thermal stability of PEG membrane by the incorporation of MYNS. Notably, both the pure PEG

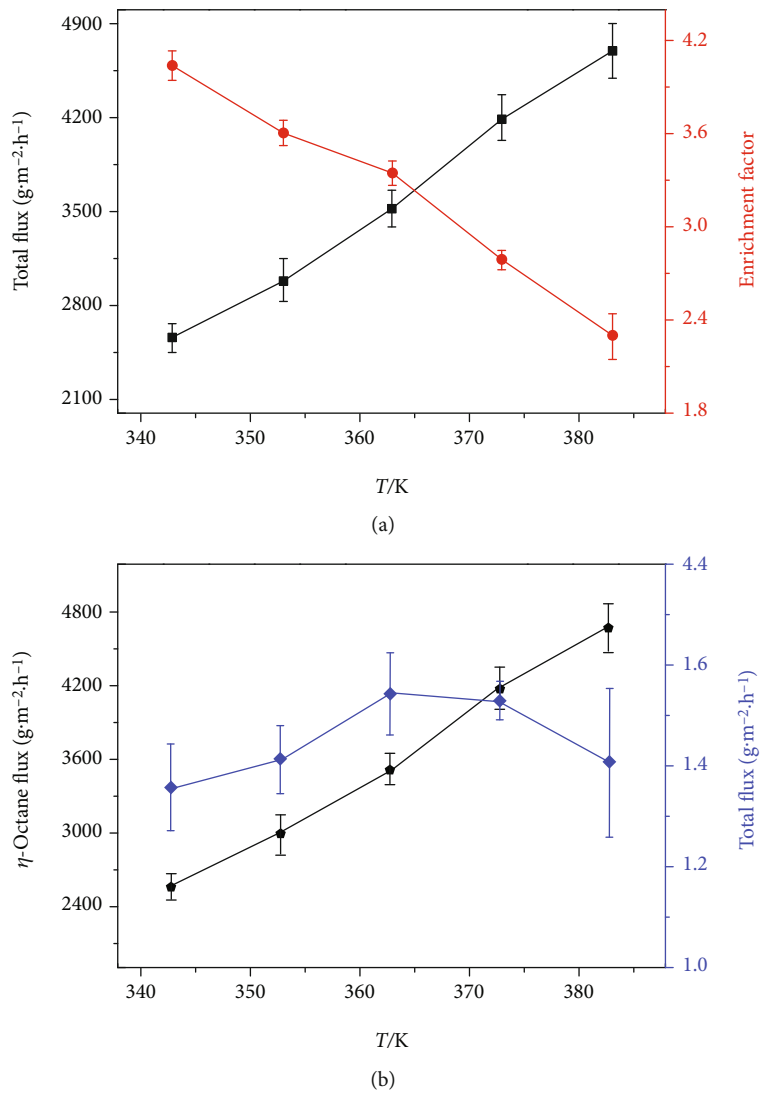

Figure 12: Effect of feed temperature on (a) total flux and enrichment factor, (b) thiophene flux, and *n*-octane flux of PEG/MYNS MMMs.

membrane and PEG/MYNS MMM start to decompose at about 390°C. It is inferred that the membranes are thermally stable below 390°C. Therefore, the thermal stability of the obtained PEG/MYNS MMMs can completely satisfy the requirement of a PV operation for gasoline desulfurization.

3.3. PV Performance of Membranes

3.3.1. Effect of MYNS Content. The effect of MYNS content on the permeation flux and enrichment factor of PEG/MYNS MMMs was investigated using a thiophene concentration in feed of 500 $\mu g \cdot g^{-1}$ and keeping operation at a temperature of 343 K. The obtained result is plotted in Figure 10. Obviously, the permeation flux keeps an upward tendency, whereas the sulfur enrichment factor presents a parabolic increment with the temperature rising. When the content of MYNS is 3 wt. %, the permeation flux is 2587 $g \cdot m^{-2} \cdot h^{-1}$, which is about two times that of the pristine PEG membrane (1355 $g \cdot m^{-2} \cdot h^{-1}$). Total flux gains are primarily attributed to the augment of the accessible free volume within membranes due to the incorporation of MYNS, which includes the intermolecular spacing between the polymer chains, interface between PEG and MYNS, and the pores in MYNS, therefore providing more diffusional pathways for thiophene and *n*-octane molecules transport. In addition, based on facilitated transport mechanism [30], the embedded MYNS served as facilitated transport efficacious carriers accelerates the mass transfer rate of thiophene through the reversible π-π interaction, which results in an increase in enrichment factor. However, when the embedded MYNS content exceeds 3 wt. %, enrichment factor declines due to the MYNS particle agglomeration that could create nonselective interfacial voids to foster *n*-octane transport through the membranes and cause the overlap of facilitated transport sites to weaken thiophene transport [21]. The maximum sulfur enrichment factor afforded by the PEG/MYNS MMM is 4.02 which corresponds to an MYNS content of 3 wt. %.

3.3.2. Effect of Feed Sulfur Concentration. The effect of the thiophene concentration in feed on the separation performance for the PEG/MYNS MMMs containing 3 wt. % was investigated at 343 K, and the result is summarized in

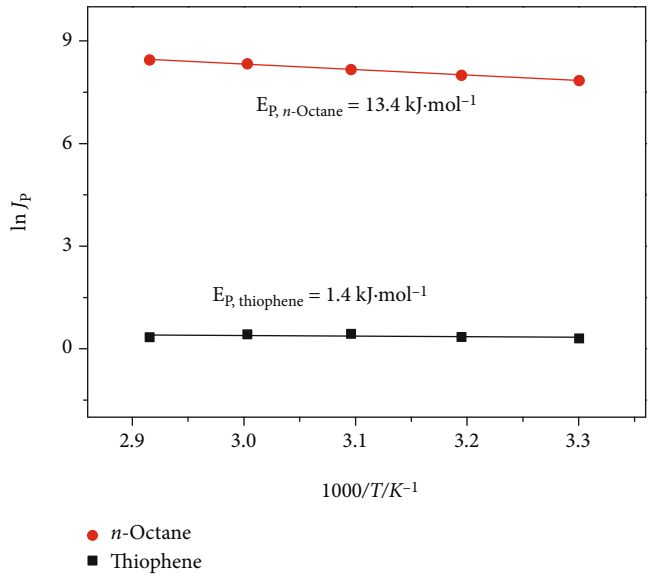

Figure 13: Arrhenius plots of thiophene and n-octane fluxes as a function of feed temperature.

Figure 11. As shown in Figure 11, permeation flux increases continuously with the increasing of the thiophene concentration within the range of 500-1700 $\mu g \cdot g^{-1}$, while the enrichment factor follows the reverse order. Because of the larger affinity of the MMMs towards thiophene, more thiophene molecules are adsorbed within the membrane with increasing of the thiophene concentration, thus exacerbating the swelling of the membrane which imparts larger polymeric interchain spacing and subsequently improves the free volume. Accordingly, the permeability of thiophene and n-octane is elevated simultaneously. Yet, given that n-octane molecules have a relatively larger kinetic diameter of about 0.63 than thiophene molecules (circa 0.53 nm) [31], the n-octane flux increases more dramatically and therefore, the selectivity towards thiophene declines. Additionally, it is known that the partial vapor pressure difference increases along with the increment of feed concentration, therefore improving the transport driving force for the target component through the membrane. Nevertheless, it is limited by the fact that the thiophene concentration in feed is of an exceptionally low level compared with n-octane. Therefore, the contribution from the gain of thiophene flux to the increment of the total flux is infinitesimal. Generally, for all these reasons, an increasing permeation flux but a decreasing enrichment factor is observed.

3.3.3. Effect of Feed Temperature. The effect of feed temperature on the desulfurization performance of PEG/MYNS MMMs containing 3 wt. % with a 500 $\mu g \cdot g^{-1}$ thiophene and n-octane solution is shown in Figure 12. It can be seen that the permeation flux increases with a trend of continuous enlargement over a temperature range from 343 to 383 K. This result mainly derived from the following: (i) the enhanced chain mobility of PEG, increasing the fractional free volume in the membrane [22], (ii) the improved saturated vapor pressure difference between the feed and permeate sides because of the elevation of vapor pressure on the feed side, increasing the transport driving force [23], and (iii) the accelerated molecular diffusivity [32]. On the contrary, the sulfur enrichment factor decreases monotonically with rising the feed temperature. The amplitude of thiophene increment, as depicted in Figure 12(b), is appreciably lower than that of n-octane, which weakened its contribution to total flux, resulting in a significant decrement in sulfur enrichment factor.

The correlation between thiophene and octane fluxes and feed temperature can be expressed by Arrhenius equation as follows:

$$J_P = A_P \exp\left(\frac{-E_P}{RT}\right), \tag{4}$$

where J_P, A_i, E_P, T, and R represent the thiophene or n-octane flux, preexponential factor, apparent activation energy, feed temperature, and gas constant, respectively. Figure 13 plots ln J_P versus 1000/T. It can be found that there is a favorable linear relationship between them. On the basis of the slope of the fitted straight lines, the apparent activation energy of n-octane calculated is 13.4 kJ·mol^{-1}, which is nine to ten times that of thiophene of 1.4 kJ·mol^{-1}. It is confirmed that the permeation of n-octane is more sensitive to the feed temperature than that of thiophene. This is consistent with the results of the considerable increase in the permeation flux of n-octane but inconspicuous variation in that of thiophene as the feed temperature goes from 343 to 383 K. As a result, a growing permeation flux but a declining enrichment factor was achieved.

3.4. Comparison of PV Desulfurization Performance with Other Reported Membranes. The PV performance of the PEG/MYNS MMMs achieved in this work and the other reported membranes for gasoline desulfurization is gathered in Table 1. Compared to other MMMs from the literature for PV desulfurization, the resulting PEG/MYNS MMM

Table 1: PV desulfurization performance of the PEG/MYNS MMMs and other membranes reported in the literature.

Membrane	Feed composition	Sulfur content ($\mu g \cdot g^{-1}$)	Feed temperature (K)	Flux ($g \cdot m^{-2} \cdot h^{-1}$)	Enrichment factor	Reference
PEG@ZIF-8/PVDF	Thiophene/*n*-heptane	800	350.15	780	7.6	[14]
PDMS/MIL-101	Thiophene/*n*-heptane	600	303.15	5200	5.6	[33]
PDMS/CuBTC	Thiophene/*n*-heptane	500	313.15	6470	5.2	[34]
PDMS–DAAg/PSf	Thiophene/*n*-heptane	500	313.15	8220	5.03	[35]
PDMS/graphene	Thiophene/*n*-heptane	500	323.15	8760	4.42	[23]
PDMS/AgY	Thiophene/*n*-heptane	—	323.15	8150	3.5	[36]
PEG/CuY	FCC gasoline fraction	1190	383.15	3190	2.95	[37]
PP/PE/alumina	Diesel fuels	—	313.15	3820	1.71	[13]
PUU	Refinery naphtha	439	348.15	85	5.12	[38]
PI (6FDA–MDA)	Thiophene/*n*-heptane	1028	350.15	1680	3.12	[39]
PI (Matrimid 5218)	Refinery naphtha	826	351.15	900	1.72	[38]
PERVAP1060	Refinery naphtha	920	347.15	5000	0.56	[38]
PEG	FCC gasoline fraction	535	383.15	640	4.83	[40]
PEG/PES	FCC gasoline	780	373.15	980	3.27	[41]
PEG/MYNs	Thiophene/*n*-octane	500	343.15	2587	4.02	This study

possesses good and acceptable comprehensive performance although it does not have the highest permeation flux or the highest sulfur enrichment factor. In addition, it can be found that its overall desulfurization performance obviously outperforms those of other pure polymeric membranes reported. Accordingly, it is inferred that the PEG/MYNS MMMs may be prospective membrane materials for practical pervaporative desulfurization application.

4. Conclusion

In this work, MYNS was prepared and doped into the PEG matrix to prepare MMMs which were utilized in the desulfurization of model gasoline by PV. The results manifest that the MYNS particles have high interfacial compatibility with the PEG matrix, and the incorporation of MYNS endows the PEG membrane with improved swelling resistance. Moreover, the as-prepared MMMs filled with MYNS showed thiophene-selective, and the overall PV performance in terms of both permeability and selectivity is enhanced for the thiophene removal from *n*-octane as compared to the pure PEG membrane. The MMMs containing 3 wt. % MYNS deliver the highest sulfur enrichment factor of 4.02 coupled with a total permeation flux of 2587 $g \cdot m^{-2} \cdot h^{-1}$ when separating the 500 $\mu g \cdot g^{-1}$ thiophene-containing *n*-octane solution at 343 K. In addition, the total permeation flux is improved as increasing the thiophene concentration in feed and feed temperature, whereas the enrichment factor decreases all along. This work may provide useful insights of MMMs for practical gasoline desulfurization applications.

Data Availability

The data used to support the findings of this study are included within the article.

Conflicts of Interest

The authors declare that they have no conflicts of interest.

Acknowledgments

The authors acknowledge the financial supported by the National Natural Science Foundation of China (No. 51903138), the Natural Science Foundation of Fujian Province (Nos. 2020J01380 and 2020J01381), the National College Students' Innovation and Entrepreneurship Training Program in China (No. 202211311018), the Foundation of Science and Technology on Sanming Institute of Fluorochemical Industry (No. FCIT20171212), the Sanming Science and Technology Project (No. 2020-G-59), and the

Scientific Research Foundation for Introducing Talent of Sanming University (contract grant number 18YG05).

References

[1] I. Babich and J. A. Moulijn, "Science and technology of novel processes for deep desulfurization of oil refinery streams: a review☆," *Fuel*, vol. 82, no. 6, article S0016-2361(02)00324-1, pp. 607–631, 2003.

[2] A. Tanimu and K. Alhooshani, "Advanced hydrodesulfurization catalysts: a review of design and synthesis," *Energy & Fuels*, vol. 33, no. 4, pp. 2810–2838, 2019.

[3] D. Mitra, "Desulfurization of gasoline by pervaporation," *Separation & Purification Reviews*, vol. 41, no. 2, pp. 97–125, 2012.

[4] S. Brunet, D. Mey, G. Pérot, C. Bouchy, and F. Diehl, "On the hydrodesulfurization of FCC gasoline: a review," *Applied Catalysis A: General*, vol. 278, no. 2, article S0926860X04008397, pp. 143–172, 2005.

[5] Y. Kong, L. Lin, J. Yang et al., "FCC gasoline desulfurization by pervaporation: effects of gasoline components," *Journal of Membrane Science*, vol. 293, no. 1-2, article S0376738807000701, pp. 36–43, 2007.

[6] M. Jain and S. K. Gupta, "Desulfurization of FCC gasoline by using spiral wound pervaporation module: removal of different types of sulfur containing species," *Chemical Engineering Research and Design*, vol. 136, article S0263876218302387, pp. 105–118, 2018.

[7] H. R. Mortaheb, F. Ghaemmaghami, and B. Mokhtarani, "A review on removal of sulfur components from gasoline by pervaporation," *Chemical Engineering Research and Design*, vol. 90, no. 3, article S0263876211002759, pp. 409–432, 2012.

[8] M. Kazemimoghadam and N. Sadeghi, "Use of polymer membranes for modeling desulfurization in the process of pervaporation through artificial neural network," *Journal of Applied Chemical Science*, vol. 5, no. 1, pp. 383–387, 2018.

[9] Y. F. Hou, H. P. Li, E. J. Liu, Y. Xu, C. Jiang, and Q. S. Niu, "Preparation and performance of thermoplastic polyurethane pervaporation membrane for gasoline desulfurization," *Gao Xiao Hua Xue Gong Cheng Xue Bao/Journal of Chemical Engineering of Chinese Universities*, vol. 32, pp. 646–652, 2018.

[10] M. K. Mishra and M. Jain, "Removal of sulfur-containing compounds from Fluid Catalytic Cracking unit (FCC) gasoline by pervaporation process: effects of variations in feed characteristics and mass transfer properties of the membrane," *Asia-Pacific Journal of Chemical Engineering*, vol. 16, no. 4, article e2653, 2021.

[11] A. Bhattacharya, P. Tondon, and M. Jain, "Modeling and Simulations of Plate and Frame Pervaporative Module for the Production of Low Sulfur Containing FCC Gasoline," *Materials Today: Proceedings*, vol. 50, pp. 146–149, 2022.

[12] A. Abdali, M. Mahmoudian, and E. Nozad, "Desulfurization of a model fuel using pervaporation membranes containing Zn-MOFs," *Journal of Polymer Research*, vol. 28, no. 7, article 271, 2021.

[13] S. H. Esmaeili-Faraj, A. Hassanzadeh, F. Shakeriankhoo, S. Hosseini, and B. Vaferi, "Diesel fuel desulfurization by alumina/polymer nanocomposite membrane: experimental analysis and modeling by the response surface methodology," *Chemical Engineering and Processing - Process Intensification*, vol. 164, article 108396, Article ID S0255270121000982, 2021.

[14] H. Sun, Z. Magnuson, W. He et al., "PEG@ZIF-8/PVDF nanocomposite membrane for efficient pervaporation desulfurization via a layer-by-layer technology," *ACS Applied Materials & Interfaces*, vol. 12, no. 18, pp. 20664–20671, 2020.

[15] R. A. Amaral, A. C. Habert, and C. P. Borges, "Activated carbon polyurethane membrane for a model fuel desulfurization by pervaporation," *Materials Letters*, vol. 137, article S0167577X14017194, pp. 468–470, 2014.

[16] F. Wu, Y. Cao, H. Liu, and X. Zhang, "High-performance UiO-66-NH_2 tubular membranes by zirconia-induced synthesis for desulfurization of model gasoline via pervaporation," *Journal of Membrane Science*, vol. 556, article S037673881830139X, pp. 54–65, 2018.

[17] Z. Yin, H. Li, H. Li et al., "Single-layer MoS2phototransistors," *ACS Nano*, vol. 6, no. 1, pp. 74–80, 2012.

[18] G. Deokar, D. Vignaud, R. Arenal, P. Louette, and J. F. Colomer, "Synthesis and characterization of MoS2 nanosheets," *Nanotechnology*, vol. 27, no. 7, article 075604, 2016.

[19] X. Li and H. Zhu, "Two-dimensional MoS2: properties, preparation, and applications," *Journal of Materiomics*, vol. 1, no. 1, article S2352847815000040, pp. 33–44, 2015.

[20] H. Li, K. Yu, X. Lei et al., "Synthesis of the MoS2@CuO heterogeneous structure with improved photocatalysis performance and H2O adsorption analysis," *Dalton Transactions*, vol. 44, no. 22, pp. 10438–10447, 2015.

[21] F. Pan, H. Ding, W. Li et al., "Constructing facilitated transport pathway in hybrid membranes by incorporating MoS_2 nanosheets," *Journal of Membrane Science*, vol. 545, article S0376738817326376, pp. 29–37, 2018.

[22] S. Yu, Z. Jiang, S. Yang et al., "Highly swelling resistant membranes for model gasoline desulfurization," *Journal of Membrane Science*, vol. 514, article S0376738816303313, pp. 440–449, 2016.

[23] D. Yang, S. Yang, Z. Jiang et al., "Polydimethyl siloxane-graphene nanosheets hybrid membranes with enhanced pervaporative desulfurization performance," *Journal of Membrane Science*, vol. 487, article S0376738815002665, pp. 152–161, 2015.

[24] P. Peng, Y. Lan, Q. Zhang, and J. Luo, "Application of graphene structure/polyurethane membrane in pervaporative desulfurization," *Journal of Applied Polymer Science*, vol. 139, no. 3, article 51514, 2022.

[25] W. Zhang, X. Ji, Z. Qin, M. Yu, W. Zhang, and J. Liu, "2D MoS2/graphene composites with excellent full Ku band microwave absorption," *RSC Advances*, vol. 6, no. 108, pp. 106187–106193, 2016.

[26] A. Mangeli, A. Mostafavi, T. Shamspur, F. Fathirad, and F. Mehrabi, "Decontamination of fenitrothion from aqueous solutions using rGO/MoS2/Fe3O4 magnetic nanosorbent: synthesis, characterization and removal application," *Journal of Environmental Health Science and Engineering*, vol. 19, no. 2, article 706, pp. 1505–1511, 2021.

[27] L. N. Long, P. T. Thi, P. Trung Kien et al., "Controllable synthesis of MoS_2/graphene low-dimensional nanocomposites and their electrical properties," *Applied Surface Science*, vol. 504, article S0169433219330090, p. 144193, 2020.

[28] P. Zhao, M. Ni, Y. Xu et al., "A novel ultrasensitive electrochemical quercetin sensor based on MoS_2 - carbon nanotube @ graphene oxide nanoribbons / HS-cyclodextrin / graphene quantum dots composite film," *Sensors and Actuators B:*

Chemical, vol. 299, article 126997, Article ID S0925400519311967, 2019.

[29] A. Gonciaruk, K. Althumayri, W. J. Harrison, P. M. Budd, and F. R. Siperstein, "PIM-1/graphene composite: a combined experimental and molecular simulation study," *Microporous and Mesoporous Materials*, vol. 209, article S1387181114003576, pp. 126–134, 2015.

[30] X. Cheng, F. Pan, M. Wang et al., "Hybrid membranes for pervaporation separations," *Journal of Membrane Science*, vol. 541, article S0376738817313595, pp. 329–346, 2017.

[31] Y. Zhang, J. Song, J. Q. Mayta et al., "Enhanced desulfurization performance of hybrid membranes using embedded hierarchical porous SBA-15," *Frontiers of Chemical Science and Engineering*, vol. 14, no. 4, article 1830, pp. 661–672, 2020.

[32] K. Cao, Z. Jiang, X. Zhang et al., "Highly water-selective hybrid membrane by incorporating g-C_3N_4 nanosheets into polymer matrix," *Journal of Membrane Science*, vol. 490, article S0376738815003816, pp. 72–83, 2015.

[33] S. Yu, F. Pan, S. Yang et al., "Enhanced pervaporation performance of MIL-101 (Cr) filled polysiloxane hybrid membranes in desulfurization of model gasoline," *Chemical Engineering Science*, vol. 135, article S0009250914007131, pp. 479–488, 2015.

[34] S. Yu, Z. Jiang, H. Ding et al., "Elevated pervaporation performance of polysiloxane membrane using channels and active sites of metal organic framework CuBTC," *Journal of Membrane Science*, vol. 481, article S0376738815000721, pp. 73–81, 2015.

[35] G. Liu, T. Zhou, W. Liu et al., "Enhanced desulfurization performance of PDMS membranes by incorporating silver decorated dopamine nanoparticles," *Journal of Materials Chemistry A*, vol. 2, no. 32, pp. 12907–12917, 2014.

[36] R. Qi, Y. Wang, J. Chen, J. Li, and S. Zhu, "Removing thiophenes from _n_ -octane using PDMS-AgY zeolite mixed matrix membranes," *Journal of Membrane Science*, vol. 295, no. 1-2, article S037673880700155X, pp. 114–120, 2007.

[37] L. Lin, Y. Zhang, and H. Li, "Pervaporation and sorption behavior of zeolite-filled polyethylene glycol hybrid membranes for the removal of thiophene species," *Journal of Colloid and Interface Science*, vol. 350, no. 1, article S0021979710006909, pp. 355–360, 2010.

[38] L. S. White, R. F. Wormsbecher, and M. Lesemann, "Membrane separation for sulfur reduction," 2004, Patent US 0211706 A1 (https://www.freepatentsonline.com/y2003/0173255.html).

[39] L. Wang, Z. Zhao, J. Li, and C. Chen, "Synthesis and characterization of fluorinated polyimides for pervaporation of _n_ -heptane/thiophene mixtures," *European Polymer Journal*, vol. 42, no. 6, article S0014305706000073, pp. 1266–1272, 2006.

[40] L. Lin, Y. Kong, G. Wang, H. Qu, J. Yang, and D. Shi, "Selection and crosslinking modification of membrane material for FCC gasoline desulfurization," *Journal of Membrane Science*, vol. 285, no. 1-2, article S0376738806005655, pp. 144–151, 2006.

[41] L. Lin, G. Wang, H. Qu et al., "Pervaporation performance of crosslinked polyethylene glycol membranes for deep desulfurization of FCC gasoline," *Journal of Membrane Science*, vol. 280, no. 1-2, article S0376738806001463, pp. 651–658, 2006.